

## IR-active phonons of the LiNbGeO<sub>5</sub> superionic crystal

© V.A. Yakovlev<sup>1</sup>, N.N. Novikova<sup>1</sup>, A.D. Molchanova<sup>1</sup>, V.A. Chernyshev<sup>2</sup>, S.A. Klimin<sup>1,¶</sup>

<sup>1</sup> Institute of Spectroscopy, Russian Academy of Sciences, Troitsk, Moscow, Russia

<sup>2</sup> Ural Federal University after the first President of Russia B.N. Yeltsin, Yekaterinburg, Russia

¶ E-mail: klimin@isan.troitsk.ru

Received April 24, 2024

Revised April 24, 2024

Accepted May 20, 2024

The infrared (IR) reflectance spectra of the LiNbGeO<sub>5</sub> superionic crystal have been studied. The crystal belongs to the orthorhombic syngony, the space group *Pnma*. Measurements in polarized light made it possible to separate phonons by symmetry in accordance with the selection rules. The spectral dependences of the reflectivity  $R(\nu)$  for three polarizations along the crystallographic axes were modeled using dispersion analysis. The parameters of IR-active phonons of symmetry  $B_{1u}$ ,  $B_{2u}$  and  $B_{3u}$  are obtained. A group-theoretical analysis of the vibrational spectrum has been performed. The frequency dependences of the complex dielectric constant and the loss function are calculated. The frequencies of IR-active phonons are calculated from the first principles. The experimental and calculated frequencies of IR-active phonons are close to each other. Inverted phonons have been detected.

**Keywords:** LiNbGeO<sub>5</sub>, IR reflection spectroscopy, dispersion analysis, first principles calculation, group-theoretic analysis.

DOI: 10.61011/PSS.2024.06.58710.103

### 1. Introduction

Lithium niobium germanate LiNbGeO<sub>5</sub> is a multifunctional material. On the one hand, it is a laser medium, and on the other hand, it is an ion conductor. LiNbGeO<sub>5</sub> was synthesized for the first time in 1985 [1] as a new compound during the study of phase relationships in the system of Li<sub>2</sub>O–Nb<sub>2</sub>O<sub>5</sub>–GeO<sub>2</sub>. LiNbGeO<sub>5</sub> has a crystal structure similar to that of the mineral sillimanite Al<sub>2</sub>SiO<sub>5</sub> [2] and crystallizes in the centrosymmetric orthorhombic space group  $D_{2h}^{16}$  (*Pnma*, № 62) [1,3–5]. The assumption of the isomorphic occurrence of Nb and Ge in one structural position turned out to be interesting [1]. In this case, niobium partially occupies the positions of germanium (up to 15%) and vice versa. This assumption was questioned in the paper [6]. 7% substitution was reported in papers [5,7].

Further studies showed that LiNbGeO<sub>5</sub> is an attractive nonlinear  $\chi^{(3)}$  material for the implementation of solid-state laser converters in the visible, near and mid-infrared (IR) spectral ranges [5,8]. In particular, experiments on stimulated Raman light scattering with picosecond pump radiation at a wavelength near 1  $\mu$ m allowed to obtain the generation of multiple stokes and anti-stokes components in an LiNbGeO<sub>5</sub> crystal with a total nonlinear optical conversion efficiency of minimum 50%. The spectroscopic and laser properties of LiNbGeO<sub>5</sub> crystals doped with chromium [5,7] were also studied. The generation was obtained at the wavelength of 1.4  $\mu$ m (Cr<sup>4+</sup>) at room temperature; it was possible to expand the generation range to 1.3–1.52  $\mu$ m at cooling the crystal [5].

An important property of the LiNbGeO<sub>5</sub> crystal is the presence of ionic conductance. The ionic conductance was calculated in Ref. [9], as part of density functional theory for almost a hundred lithium-containing crystalline compounds. LiNbGeO<sub>5</sub> fell into the group of crystals with the highest ionic conductance. Experiments were carried out in Ref. [10,11] to study ionic conductance in LiNbGeO<sub>5</sub>. The measured value  $\sigma_a(570\text{ K}) = 2 \cdot 10^{-5}$  S/cm corresponds to superionic conductance. It was found that the direction along the a-axis is the most favorable for lithium diffusion, since it is characterized by the lowest activation energy, as well as the presence of additional interstitial positions. LiNbGeO<sub>5</sub> is a new material with high durability that is promising for use as an anode for lithium-ion batteries according to [12].

Information on the phonon spectrum is important for studying both relaxation processes and the dynamics of lithium participation in conductance. The information on the vibrational properties of the compound under study is incomplete in the scientific literature. The Raman spectra in LiNbGeO<sub>5</sub> are given in [5,6]. As far as we know, there is no information on IR phonons in the literature. Therefore, we studied the IR reflectance spectra of the LiNbGeO<sub>5</sub> crystal and performed an ab initio calculation of the phonon spectrum.

### 2. Research methods

Transparent crystals of LiNbGeO<sub>5</sub> were grown using the Czochralski method from a stoichiometric melt at the Faculty of Physics of the Lomonosov Moscow State

University. A crystal with the size of approximately  $6 \times 6 \times 6 \text{ mm}^3$  was cut out for optical studies with the edges perpendicular to the crystallographic axes.

Infrared reflectance spectra were measured in s-polarization at room temperature using Bruker IFS 66 Fourier spectrometer with a reflectance attachment at an incidence angle close to the normal ( $13^\circ$ ). A polyethylene polarizer with a wire grid was used for polarization of the incident beam in the far IR region of the spectrum ( $50\text{--}700 \text{ cm}^{-1}$ ) and a polarizer based on a KRS-5 crystal (TiBr–TII solid solution) was obtained in the mid-IR region (over  $450 \text{ cm}^{-1}$ ). Interferograms were recorded using pyroelectric detectors based on DTGS (deuterated triglycine sulfate). Weak phonons were registered in the low-frequency region using BRUKER IFS125HR Fourier spectrometer with a germanium bolometer operating at helium temperatures.

Dispersion analysis of reflection spectra was used [13] to calculate dielectric permittivity. The spectra were approximated using the model of independent Lorentz oscillators using the programs SCOUT [14,15] and RefFIT [16]. The frequency-dependent reflectivity  $R(\nu)$  was calculated using the Fresnel formulas. Then the standard deviation of the calculated spectrum from the experimental one was minimized. In this case, the complex dielectric permittivity was represented as the sum of contributions  $N$  of evanescent oscillators

$$\varepsilon(\nu) = \varepsilon_\infty + \sum_{j=1}^N \frac{\Delta\varepsilon_j \nu_{\text{TO}j}^2}{\nu_{\text{TO}j}^2 - \nu^2 + i\gamma_j \nu}. \quad (1)$$

Here  $\nu_{\text{TO}j}$ ,  $\Delta\varepsilon_j$  and  $\gamma_j$  are a transverse oscillation (TO) frequency, oscillator strength and decay of the  $j$ th phonon;  $\varepsilon_\infty$  — high frequency dielectric permittivity. The strength of the oscillator is related by a simple relationship with the parameter  $\nu_p$ , called the plasma frequency and used by a number of researchers,  $\Delta\varepsilon_j \nu_{\text{TO}j}^2 = \nu_p^2$ .

Ab initio calculations were performed within the density functional theory (DFT) with the use of hybrid functionals B3LYP, which incorporate the contribution of nonlocal exchange in the Hartree–Fock formalism. The CRYSTAL17 [17,18] program was used, designed for simulating periodic structures as part of the approach „molecular orbital — linear combination of atomic orbitals“. For lithium, germanium and oxygen, all-electron basis sets were used, available on the CRYSTAL program website as Li\_5–11(1d)G\_baranek\_2013\_LiNbO<sub>3</sub>, Ge\_pob\_TZVP\_2012 and O\_8–411(1d)G\_baranek\_2013\_PbZrO<sub>3</sub> [18]. A pseudopotential was used for the description of the inner shells of niobium, in which its outer shells ( $4s^2 4p^6$ ), involved in chemical bonding, were described by the valence basis set. This pseudopotential with the attached valence basis set is available as Nb\_SC\_HAYWSC–31(31d)G\_baranek\_2013\_LiNbO<sub>3</sub> at the program website.

The accuracy of self-consistency field calculation in solving a system of one-electron Kohn–Sham equations

was set to  $10^{-9}$  a.u. The accuracy of two-electron integral calculation was minimum than  $10^{-8}$  a.u. Integration over the Brillouin zone was carried out using the Monkhorst–Pack of  $k$ -point grid  $12 \times 12 \times 12$ .

### 3. Crystal structure of LiNbGeO<sub>5</sub> and group-theoretical analysis

The space symmetry group  $D_{2h}^{16}$  allows for several different settings. In particular, the  $Pbnm$  setting is used to describe the structure in Ref. [1]. We use the  $Pnma$  setting in this paper which standard for this group, in which the axes are designated differently from the  $Pbnm$  setting (cyclic rearrangement of axes). Fragment of crystal structure LiNbGeO<sub>5</sub> is shown in Figure 1. The figure was created using the program Balls and Sticks [19]. Nb and Ge atoms are localized in planes of mirror symmetry in positions  $4c$ , while Li atoms are localized in inversion centers  $4a$ . Li and Nb atoms have an octahedral oxygen environment, and Ge atoms are located in oxygen tetrahedra. It is possible to identify chains of LiO<sub>6</sub> octahedra linked by vertices along the  $b$  axis ( $a$  in the  $Pbnm$  unit) in the crystal structure of LiNbGeO<sub>5</sub>, and columns of NbO<sub>6</sub> octahedra linked to each other through a common edge in the direction of the  $b$  axis (respectively,  $c$  in the  $Pbnm$  [1,5] unit). The GeO<sub>4</sub> tetrahedra do not share any atoms with each other. They link chains of lithium and columns of niobium octahedra.

The primitive rhombic cell of the crystal of LiNbGeO<sub>5</sub> contains four formula units, i.e. 32 atoms, possessing 96 degrees of freedom and the same number of normal vibrational modes. Knowing the positions of atoms in the structure LiNbGeO<sub>5</sub> [1,5] and using tables from the work of Porto [20], we carried out a factor group analysis. As a result, minus the three acoustic modes  $B_{1u} + B_{2u} + B_{3u}$ , the following expression for the optical vibrational modes

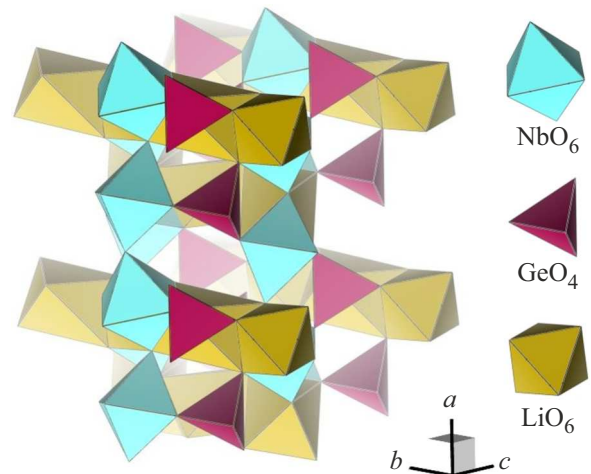


Figure 1. Fragment of crystal structure LiNbGeO<sub>5</sub>.

**Table 1.** Parameters of IR-active vibrational modes of a crystal of symmetry  $B_{1u}$ : calculated  $\nu_{\text{TO,calc}}$  and obtained from experiment frequencies of transverse and longitudinal oscillations  $\nu_{\text{TO,exp}}$  and  $\nu_{\text{LO,exp}}$ , oscillator strength  $\Delta\varepsilon$  and decay constants  $\gamma$

Calculation	Experiment			
$\nu_{\text{TO,calc}}, \text{cm}^{-1}$	$\nu_{\text{TO,exp}}, \text{cm}^{-1}$	$\nu_{\text{LO,exp}}, \text{cm}^{-1}$	$\Delta\varepsilon$	$\gamma, \text{cm}^{-1}$
117	131	131.1	0.03	6
146	150*	150.2	0.02	19
175	181	181.7	0.03	9
189	210	210.6	0.06	8.5
259	253*	255	0.03	12
332	276	284	0.8	21
362	350	355	0.58	20
400	413	455	3.06	13
430	453	466	0.1	22
457	469	492	0.09	11
505	510	552	0.34	40
712	733	775	0.74	17
808	801	836	0.18	16
885	896	920	0.15	16
961	959	989	0.09	12

Note. \* — very weak modes.

was obtained:

$$\Gamma^{\text{vibr}} = 13A_g + 11A_u + 8B_{1g} + 15B_{1u} + 13B_{2g} + 10B_{2u} + 8B_{3g} + 15B_{3u}. \quad (2)$$

$A_u$  vibrational modes are optically inactive, the remaining gerade  $g$  modes and ungerade  $u$  modes are active in the Raman light scattering (RS) and IR reflection (absorption) spectra, respectively. No vibrational mode can be active simultaneously in both IR and RS spectra due to the rule of alternative prohibition in crystals with an inversion center. The following expression is true for IR mode:

$$\Gamma^{\text{IR}} = 15B_{1u}(\mathbf{E} \parallel c) + 10B_{2u}(\mathbf{E} \parallel b) + 15B_{3u}(\mathbf{E} \parallel a). \quad (3)$$

The designations in brackets refer to the components of the electric field of electromagnetic radiation that interact with the corresponding oscillations.

## 4. Findings and discussion

Reflectivity spectra for radiation polarization along three crystallographic axes ( $a$ ,  $b$  and  $c$ ) are presented in Figure 2. The three experimental spectra clearly differ from each other, which confirms the correctness of the geometry

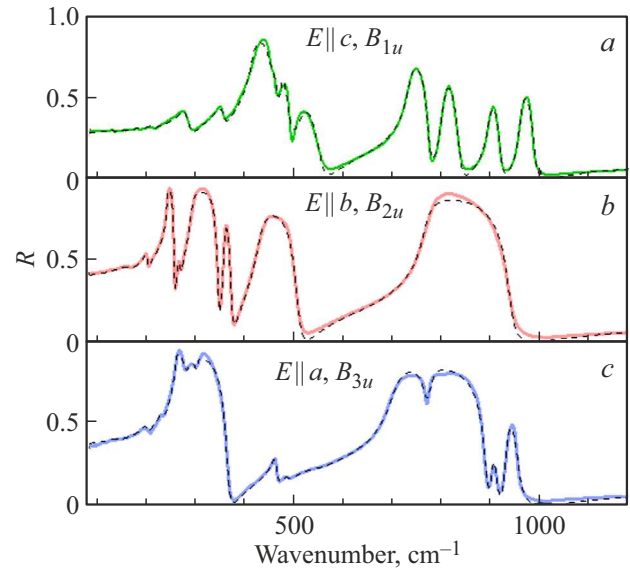


**Figure 2.** Experimental IR reflectance spectra (thick colored lines) of the LiNbGeO<sub>5</sub> crystal, for three incident light configurations. *a*) Modes  $B_{1u}$  in  $\mathbf{E} \parallel a$  polarization, *b*)  $B_{1u} - \mathbf{E} \parallel b$ , *c*)  $B_{1u} - \mathbf{E} \parallel c$ . Dashed lines — calculated spectra.

of the experiment and allows to separate the vibrational modes by their activity in accordance with the selection rules. The number of strong phonons clearly observed in Figure 2 ( $9B_{1u}$ ,  $7B_{2u}$  and  $10B_{3u}$ ) is less than expected from formula (3). Prefacing the description of the calculation presented below, let us say that it was an *ab initio* calculation data that helped us focus on a detailed study of the low-frequency spectral region in order to search for the missing phonons. The data obtained after accumulation using a sensitive far-IR bolometer are presented in Figure 3. As a result, weak phonon modes, additional to the strong ones, were experimentally detected, the TO frequencies of which correspond to the position of the dashed lines.

The reflectivity spectra were calculated as part of the model of independent Lorentz oscillators. The quantities  $\nu_j$ ,  $\Delta\varepsilon_j$ ,  $\gamma_j$  and  $\varepsilon_\infty$  in formula (1) were used as fitting parameters to minimize the root-mean-square deviation of the calculated spectrum from the experimental one. The values of frequencies, oscillator strengths and damping constants obtained as a result of the best fit are given in Tables 1, 2 and 3 for phonons of symmetry  $B_{1u}$ ,  $B_{2u}$  and  $B_{3u}$ , respectively. In this case, the values of high-frequency dielectric permittivity were  $\varepsilon_{a\infty} = 4.38$ ,  $\varepsilon_{b\infty} = 4.79$  and  $\varepsilon_{c\infty} = 4.4$ .

The phonon frequencies were calculated *ab initio* for further interpretation of the spectra. The first interval consisted of optimization of the parameters of the crystal structure. The seed data (atomic positions and lattice constants) were taken from Ref. [1]. The constant lattices LiNbGeO<sub>5</sub>  $a = 0.7966$  nm,  $b = 0.6762$  nm and  $c = 0.7552$  nm were obtained as a result of optimization. They are in good agreement with experimental literature data ( $a = 0.775$  nm,

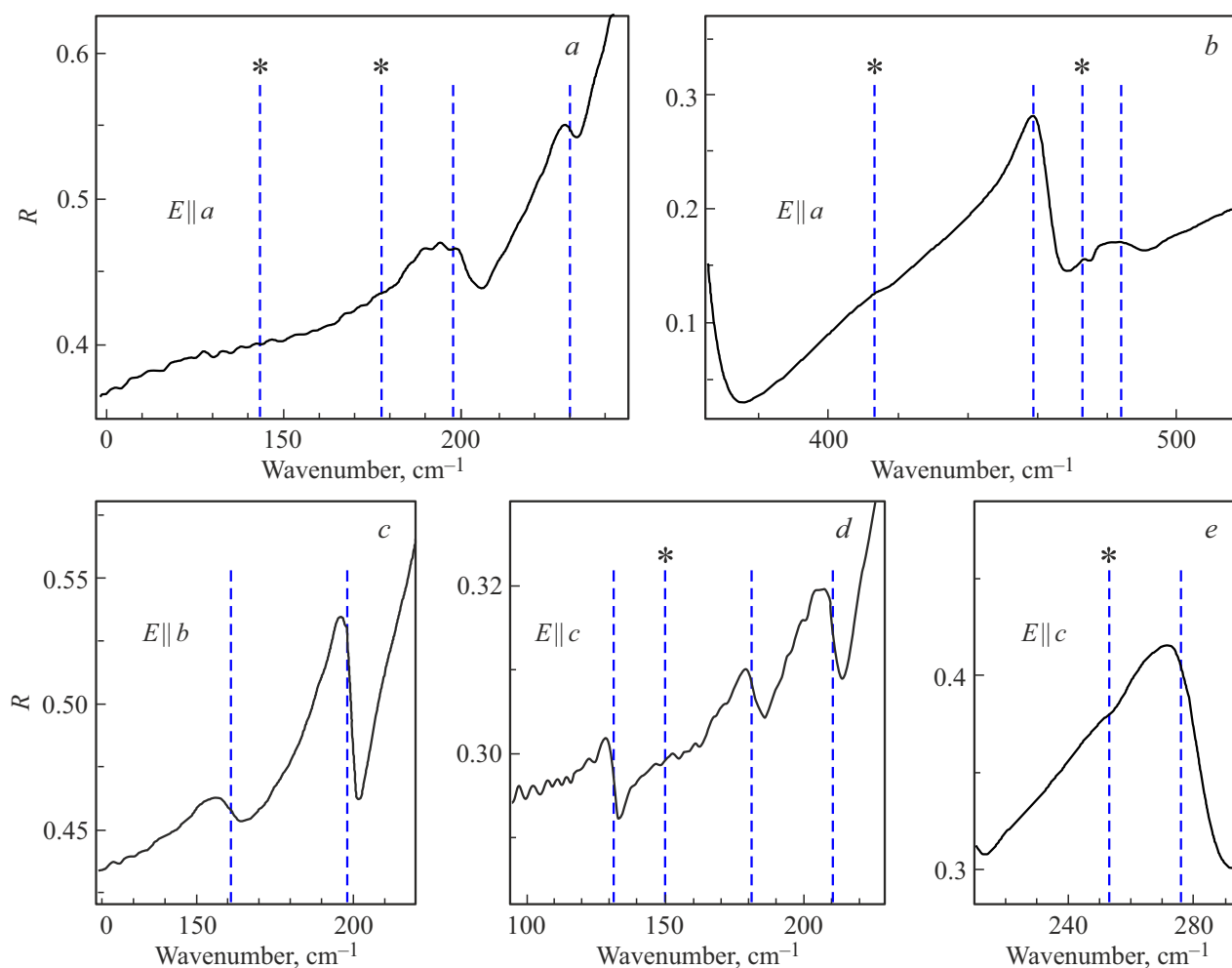


**Figure 3.** Weak vibrational IR modes in the reflection spectra of the LiNbGeO<sub>5</sub> crystal. Direction of incident light polarization: a, b) E || a, c) E || b and d, e) E || c. Vertical dashed lines indicate TO frequency positions. Asterisks indicate the weakest modes.

$b = 0.6713$  nm and  $c = 0.7522$  nm). The phonon spectrum was then calculated for the optimized crystal structure corresponding to the energy minimum. Phonon spectrum frequencies were calculated at point  $\Gamma$ . These calculations are performed in the harmonic approximation in CRYSTAL program, and a dynamical matrix is computed in the process. The first and the second derivatives with respect to ion displacements are calculated analytically and numerically, respectively [21].

The values of the frequencies of IR-active vibrational modes obtained as a result of the calculation are also given in Tables 1, 2 and 3. The number of vibrational modes found in the experiment coincides with those expected as part of factor group analysis for modes of symmetry  $B_{1u}$  and  $B_{3u}$ . For the  $B_{2u}$  symmetry it was possible to register eight experimental frequencies out of ten expected (see Table 2). The main reason for this discrepancy is apparently the very weak intensity of the two vibrational modes. The frequencies in Tables 1 and 3 marked with asterisks refer to very weak modes. These oscillations are also marked with asterisks in Figure 3. Taking

them into account allows for a significant reduction of the error in the dispersion analysis of reflection spectra. The presence of spectra well separated by polarizations indicates the good quality of the crystal and casts doubt on the assumption of disorder of the crystal structure [1,5,7] associated with the mutual substitution of germanium and niobium positions. Fifteen percent substitution means that each niobium atom, as well as germanium, will, on average, have a structural defect in the second coordination sphere. We tend to agree with the conclusions of the paper [6], the authors of which concluded that the spectra correspond to an undisturbed relationship in the distribution of ions based on an analysis of the RS of LiNbGeO<sub>5</sub>.

It can be seen that the calculated and experimental frequencies agree well for the majority of phonon modes. This is confirmed by Figure 4. The points in the figure correspond to vibrational modes of the LiNbGeO<sub>5</sub> crystal. The abscissa of the point corresponds to the experimental TO frequency, the ordinate — calculated. The deviation from the straight line  $y = x$  is not large.

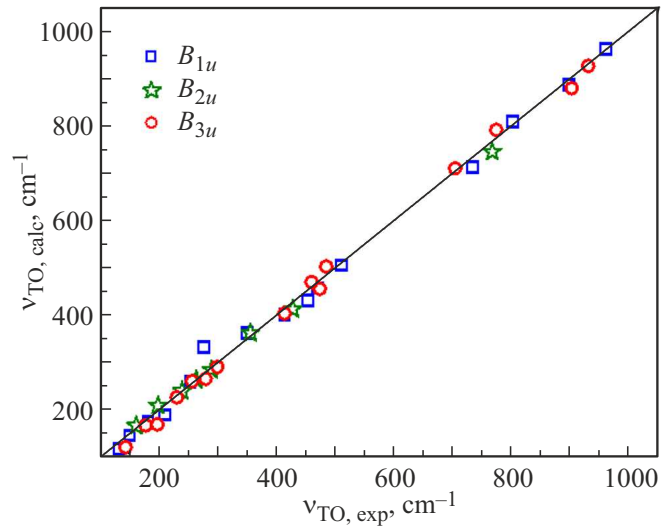
**Table 2.** Parameters of IR-active vibrational modes of a crystal of symmetry  $B_{2u}$ : calculated  $\nu_{\text{TO,calc}}$  and obtained from experiment frequencies of transverse and longitudinal oscillations  $\nu_{\text{TO,exp}}$  and  $\nu_{\text{LO,exp}}$ , oscillator strength  $\Delta\varepsilon$  and decay constants  $\gamma$ 

Calculation	Experiment			
	$\nu_{\text{TO,exp}}, \text{cm}^{-1}$	$\nu_{\text{LO,exp}}, \text{cm}^{-1}$	$\Delta\varepsilon$	$\gamma, \text{cm}^{-1}$
83	—	—	—	—
166	161	161.9	0.65	29
209	198	199.2	0.55	6.6
239	239	254.4	4.5	2.5
263	263	265.8	0.4	7.3
284	289	344.2	4.6	8
362	355	372	0.27	5.5
412	427	508.7	1.6	21
462	—	—	—	—
744	766	938	1.7	19

**Table 3.** Parameters of IR-active vibrational modes of a crystal of symmetry  $B_{3u}$ : calculated  $\nu_{\text{TO,calc}}$  and obtained from experiment frequencies of transverse and longitudinal oscillations  $\nu_{\text{TO,exp}}$  and  $\nu_{\text{LO,exp}}$ , oscillator strength  $\Delta\varepsilon$  and decay constants  $\gamma$ 

Calculation	Experiment			
	$\nu_{\text{TO,exp}}, \text{cm}^{-1}$	$\nu_{\text{LO,exp}}, \text{cm}^{-1}$	$\Delta\varepsilon$	$\gamma, \text{cm}^{-1}$
121	143*	144	0.41	40
167	177*	180	0.16	22
169	197	200	0.37	10
226	230	231	0.55	11
260	256	363	6.3	5
265	279	280	1.1	22
290	299	298**	0.05	6
403	413*	413.3	0.014	17
455	473*	486.6	0.001	3
469	459	464	0.14	11
502	484	485.5	0.045	20
709	703	889	2.4	27
790	773	768**	0.11	20
878	901	912	0.01	11
925	929	956	0.03	11

Not e. \* — very weak modes, \*\* — inverted phonons.


**Figure 4.** Correspondence plot between experimental and calculated TO frequencies of IR active vibrational modes of the LiNbGeO<sub>5</sub> crystal. Points for modes of different symmetries are indicated by different icons:  $B_{1u}$  — blue squares,  $B_{2u}$  — green stars and  $B_{3u}$  — red circles. The solid line corresponds to the straight line  $y = x$  (perfect match).

Figures 5–7 shows the spectral dependences of the real  $\varepsilon_1(\nu)$  and imaginary  $\varepsilon_2(\nu)$ , parts of the dielectric permittivity  $\varepsilon = \varepsilon_1 + i\varepsilon_2$  and the loss function (LF): calculated on the basis of the simulation:

$$\text{LF} = -\text{Im}(\varepsilon^{-1}) = \frac{\varepsilon_2}{\varepsilon_1^2 + \varepsilon_2^2}. \quad (4)$$

The dielectric constant for all polarizations has regions of negative values. They are marked with dark gray wide lines at the bottom of the drawings. Interestingly, in these regions the existence of surface polaritons (SP) becomes possible. The presence of fairly extended frequency ranges with a negative value of the dielectric constant  $\varepsilon_1$  makes it interesting to study the SP in the LiNbGeO<sub>5</sub> crystal.

The maxima in the frequency dependence of the imaginary part of the dielectric permittivity indicate the positions of the TO frequencies, while the maxima of the loss function correspond to the longitudinal LO frequencies. When the frequency of a weak mode falls within the TO–LO interval of a strong mode of the same symmetry, it appears as a dip at the top of the strong mode reflection band (residual ray band). In this case the longitudinal frequency of the weak mode may become smaller in magnitude than the transverse frequency. This phenomenon of the inverted phonons was first noticed in quartz [22,23] and is observed in other crystals, see, for example, [24]. This effect was discussed in detail in the papers of Gervais [25] and Vinogradov [26,27]. The examples of inverted phonons are shown in Figure 2, c. At the top of the strong and wide reflection band corresponding to the phonon  $B_{3u}$  with frequency  $\nu_{\text{TO}} = 703 \text{ cm}^{-1}$ , there is a dip due to the phonon  $B_{3u}$  with frequency  $\nu_{\text{TO}} = 773 \text{ cm}^{-1}$ . The TO and LO frequencies of

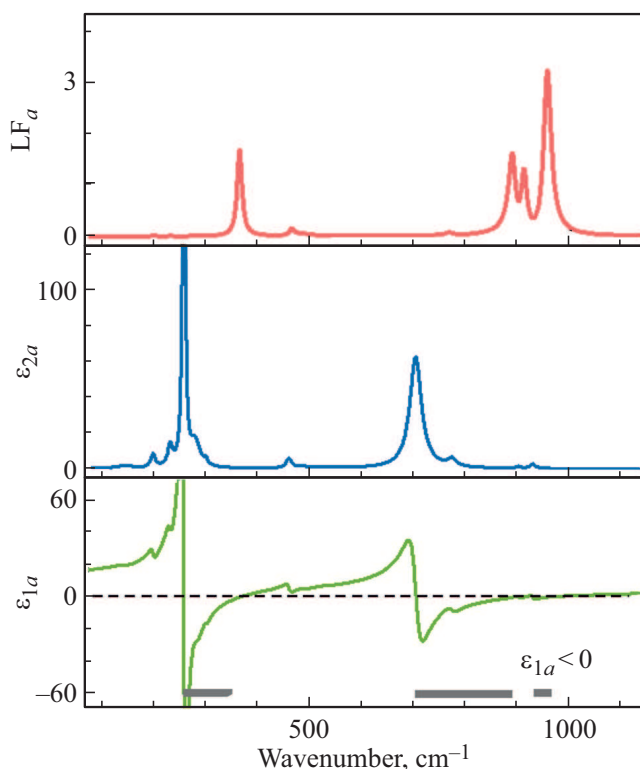


**Figure 5.** Frequency dependences of the real ( $\epsilon_{1a}$ ) and imaginary ( $\epsilon_{2a}$ ) parts of the dielectric permittivity and the loss function ( $LF_a$ ) for polarization  $\mathbf{E} \parallel a$ .

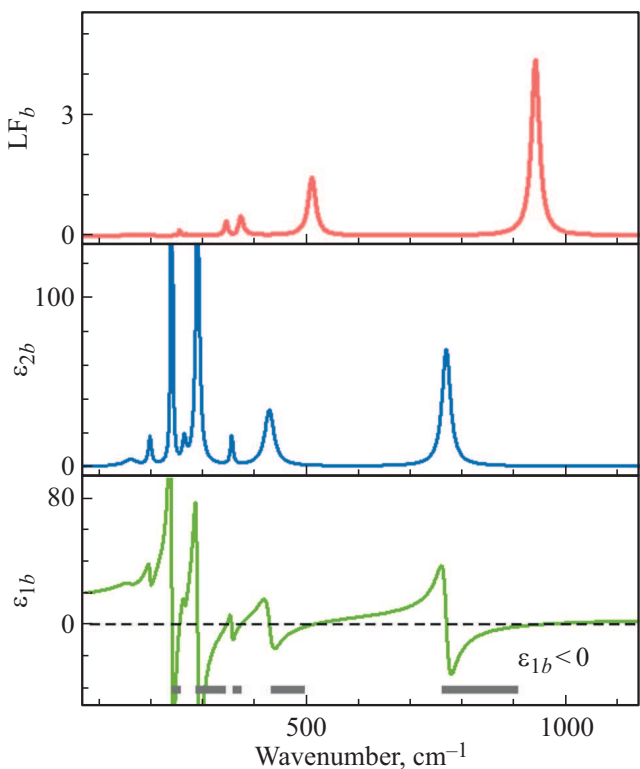


**Figure 6.** Frequency dependences of the real ( $\epsilon_{1b}$ ) and imaginary ( $\epsilon_{2b}$ ) parts of the dielectric permittivity and the loss function ( $LF_b$ ) for polarization  $\mathbf{E} \parallel b$ .

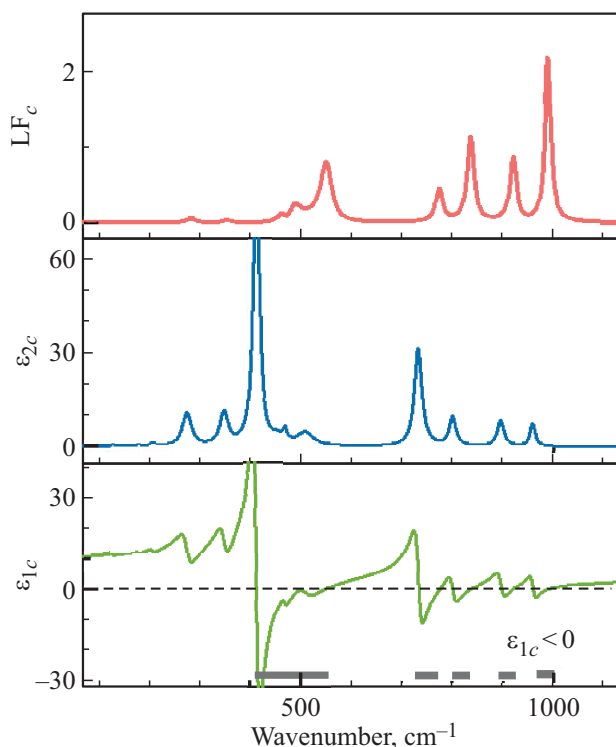


**Figure 7.** Frequency dependences of the real ( $\epsilon_{1c}$ ) and imaginary ( $\epsilon_{2c}$ ) parts of the dielectric permittivity and the loss function ( $LF_c$ ) for polarization  $\mathbf{E} \parallel c$ .

the last phonon are inverted (see Table 3). The phonon  $B_{3u}$  with frequency  $\nu_{TO} = 299 \text{ cm}^{-1}$  is also inverted.

## 5. Conclusion

The phonon spectrum of the  $\text{LiNbGeO}_5$  crystal was studied using IR spectroscopy and ab initio calculations. IR reflectance spectra were measured in polarized light. Simulating of the reflectivity spectra yielded the parameters of the phonon modes of the  $\text{LiNbGeO}_5$  crystal. A good agreement between experimental and calculated frequencies was obtained. The spectral dependences of the dielectric permittivity (imaginary and real parts) and loss functions in the IR region of the spectrum are calculated. Two inverted phonons of symmetry  $B_{2u}$  were discovered.

## Acknowledgments

The authors thank B.V. Mill for providing the sample. The work was carried out with the use of the equipment of the USU of ISAS „Multifunctional high-resolution wide-range spectroscopy“ <http://www.ckp-rf.ru/usu/508571>.

## Funding

Work of authors V.A.Ya., N.N.N. and S.A.K. carried out as part of the state assignment No. FFUU-2022-0003. V.A.Ch. thanks the project No. FEUZ-2023-0017 of the

Ministry of Education and Science RF. This study by A.D.M. was supported by grant No. 19-72-10132 from the Russian Science Foundation.

### Conflict of interest

The authors declare that they have no conflict of interest.

### References

- [1] E.L. Belokoneva, B.V. Mill, A.V. Butashin. *Kristallografiya* **30**, 2, 290 (1985). (in Russian).
- [2] E.R. Varley. *Sillimanite (Andalusite, Kyanite, Sillimanite)*. Overseas Geological Surveys, Mineral Resources Division, London (1965). 165 p.
- [3] A.A. Kaminsky, B.V. Mill, E.L. Belokoneva, A.V. Butashin. *Izv. AN SSSR. Neorgan. materialy* **27**, 9, 1899 (1991). (in Russian).
- [4] A.A. Kaminsky, A.V. Butashin, B.V. Mill. *Izv. AN SSSR. Neorgan. materialy* **25**, 9, 1052 (1989). (in Russian).
- [5] A.A. Kaminskii, H.J. Eichler, D. Grebe, R. Macdonald, J. Findeisen, S.N. Bagayev, A.V. Butashin, A.F. Konstantinova, H. Manaa, R. Moncorge, F. Bourgeois, G. Boulon. *Opt. Mater.* **10**, 4, 269 (1998).  
[https://doi.org/10.1016/S0925-3467\(98\)00010-X](https://doi.org/10.1016/S0925-3467(98)00010-X)
- [6] G. Blasse, G.J. Dirksen. *J. Solid State Chem.* **65**, 2, 283 (1986). [https://doi.org/10.1016/0022-4596\(86\)90065-4](https://doi.org/10.1016/0022-4596(86)90065-4)
- [7] R. Moncorge, H. Manaa, A.A. Kaminskii. *Chem. Phys. Lett.* **200**, 6, 635 (1992).  
[https://doi.org/10.1016/0009-2614\(92\)80102-H](https://doi.org/10.1016/0009-2614(92)80102-H)
- [8] A.A. Kaminskii, A.V. Butashin, H.J. Eichler, D. Grebe, R. Macdonald, J. Findeisen. *The XXI Reading for S.I. Vavilov's Memory*. Physical Institute of the Russian Academy of Sciences. Moscow (1997).
- [9] X. He, Q. Bai, Y. Liu, A.M. Nolan, C. Ling, Y. Mo. *Adv. Energy Mater.* **9**, 43, 1902078 (2019).
- [10] S.Yu. Stefanovich, B.V. Mill, A. Mosunov. *Abstr. 7th Int. Seminar on Ferroelastic Physics. Kazan L3* (1997).
- [11] S.Yu. Stefanovich, V.V. Fomichev, V.V. Konovalova, A.V. Mosunov, B.V. Mill. *Vestn. MITKhT* **4**, 1, 88 (2009). (in Russian).
- [12] X. Cao, Y. Cao, H. Peng, Y. Cao, H. Zhu, N. Wang, X. Dong, C. Wang, Y. Liu, J. Wu, Y. Xia. *ACS Sustainable Chem. Eng.* **9**, 35, 11883 (2021).
- [13] A.S. Barker Jr. *Phys. Rev.* **132**, 4, 1474 (1963).
- [14] W. TheiB. *The SCOUT through CAOS, Manual of the Windows application SCOUT*.
- [15] M. Krüger, S. Hilbrich, M. Thönissen, D. Scheyen, W. TheiB, H. Lüth. *Opt. Commun.* **146**, 1–6, 309 (1998).
- [16] A.B. Kuzmenko. *Rev. Scientific Instrum.* **76**, 8, 083108 (2005).
- [17] R. Dovesi. *CRYSTAL17 User's Manual*. [Electronic source]. Available at:  
<https://www.crystal.unito.it/Manuals/crystal17.pdf>
- [18] *CRYSTAL17 a computational tool for solid state chemistry and physics*. [Electronic source]. Available at:  
<http://www.crystal.unito.it/index.php>
- [19] T.C. Ozawa, S.J. Kang. *J. Appl. Cryst.* **37**, 4, 679 (2004).
- [20] D.L. Rousseau, R.P. Bauman, S.P.S. Porto. *J. Raman Spectrosc.* **10**, 1, 253 (1981).
- [21] F. Pascale, C.M. Zicovich-Wilson, F. López Gejo, B. Civalleri, R. Orlando, R. Dovesi. *J. Comput. Chem.* **25**, 6, 888 (2004).
- [22] J.F. Scott, S.P.S. Porto. *Phys. Rev.* **161**, 3, 903 (1967).
- [23] F. Gervais, B. Piriou. *Phys. Rev. B* **11**, 10, 3944 (1975).
- [24] S.A. Klimin, A.B. Kuzmenko, M.A. Kashchenko, M.N. Popova. *Phys. Rev. B* **93**, 5, 054304 (2016).
- [25] F. Gervais. *Opt. Commun.* **22**, 1, 116 (1977).
- [26] E.A. Vinogradov, B.N. Mavrin, N.N. Novikova, V.A. Yakovlev. *Phys.–Usp.* **52**, 1, 290 (2009).
- [27] E.A. Vinogradov. *Phys.–Usp.* **63**, 8, 775 (2020).

Translated by A.Akhtyamov